Pourjamal, Sara; Kataja, Mikko; Maccaferri, Nicolò; Vavassori, Paolo; van Dijken, Sebastiaan

Hybrid Ni/SiO2/Au dimer arrays for high-resolution refractive index sensing

Published in:
Nanophotonics

DOI:
10.1515/nanoph-2018-0013

Published: 01/05/2018

Document Version
Publisher's PDF, also known as Version of record

Please cite the original version:
Pourjamal, S., Kataja, M., Maccaferri, N., Vavassori, P., & Van Dijken, S. (2018). Hybrid Ni/SiO2/Au dimer arrays for high-resolution refractive index sensing. Nanophotonics, 7(5), 905-912. https://doi.org/10.1515/nanoph-2018-0013

Research article

Sara Pourjamal, Mikko Kataja, Nicolò Maccaferri, Paolo Vavassori and Sebastiaan van Dijken*

Hybrid Ni/SiO_2/Au dimer arrays for high-resolution refractive index sensing

https://doi.org/10.1515/nanoph-2018-0013
Received January 29, 2018; revised March 29, 2018; accepted April 14, 2018

Abstract: We introduce a novel magnetoplasmonic sensor concept for sensitive detection of refractive index changes. The sensor consists of a periodic array of Ni/SiO_2/Au dimer nanodisks. Combined effects of near-field interactions between the Ni and Au disks within the individual dimers and far-field diffractive coupling between the dimers of the array produce narrow linewidth features in the magneto-optical Faraday spectrum. We associate these features with the excitation of surface lattice resonances and show that they exhibit a spectral shift when the refractive index of the surrounding environment is varied. Because the resonances are sharp, refractive index changes are accurately detected by tracking the wavelength where the Faraday signal crosses 0. Compared to random distributions of pure Ni nanodisks or Ni/SiO_2/Au dimers or periodic arrays of Ni nanodisks, the sensing figure of merit of the hybrid magnetoplasmonic array is more than one order of magnitude larger.

Keywords: biosensing; magnetic nanoparticle array; magneto-optics; magnetoplasmonics.

1 Introduction

Label-free plasmonic biosensors exploit surface plasmon polaritons (SPPs) at metal/dielectric interfaces or localized surface plasmon resonances (LSPRs) in metallic nanostructures [1–5]. Both sensing approaches record molecular binding events between the target analyte and its corresponding receptor on the metal surface by monitoring shifts of the plasmon resonance condition in optical transmission or reflection spectra. The measurement sensitivity (S), often defined as the shift of the plasmon resonance peak ($\Delta\lambda$) upon small changes of the embedding medium refractive index (Δn), is especially large for SPP sensors because their slowly decaying electromagnetic field probes large volumes of the dielectric environment. On the other hand, strong confinement of electromagnetic fields to 30–40 nm above the surface of metal nanoparticles offers good surface sensitivity to local changes of the refractive index, enabling label-free molecular-level detection in LSPR-based sensors [6–9]. Other advantages of nanostructured plasmonic sensors include high spatial resolution, size-based selectivity, small footprint, and the ability to tailor the sensing performance by altering the size or shape of the metal nanostructures. Besides sensitivity, the detection limit of plasmonic biosensors depends on the resonance line width. The figure-of-merit (FoM) is usually defined as the sensitivity divided by the full width at half maximum of the plasmon resonance peak. Nanostructure design [6] and phase-sensitive detection schemes [9] can be used to enhance the sensing FoM.

Ferromagnetic metals also support the excitation of surface plasmon resonances [10–12]. In ferromagnetic nanoparticles, spin-orbit coupling results in the excitation of two LSPRs, one along the direction of the incident electric field and the second induced orthogonally to the first and the direction of magnetization [13]. The amplitude and phase relations of these two LSPRs determine the magneto-optical response of a ferromagnetic nanoparticle, i.e. the rotation and ellipticity of light polarization upon transmission or reflection. Phase-sensitive detection of the magneto-optical signal provides a sensitive method for biosensing at the molecular level, as recently demonstrated for cylindrical Ni nanoantennas [14].

Ordering of plasmonic nanoparticles into a regular array can improve the FoM. In this geometry, hybridization between LSPRs and the diffracted order of the array

***Corresponding author: Sebastiaan van Dijken,** NanoSpin, Department of Applied Physics, Aalto University School of Science, FI-00076 Aalto, Finland, e-mail: sebastiaan.van.dijken@aalto.fi.
http://orcid.org/0000-0001-6372-2252
Sara Pourjamal and Mikko Kataja: NanoSpin, Department of Applied Physics, Aalto University School of Science, FI-00076 Aalto, Finland
Nicolò Maccaferri: Istituto Italiano di Tecnologia, Via Morego 30, 16163 Genova, Italy
Paolo Vavassori: CIC nanoGUNE, E-20018 Donostia-San Sebastian, Spain; and Ikerbasque, Basque Foundation for Science, E-48013 Bilbao, Spain

produces narrow line width surface lattice resonances (SLRs) in transmittance and reflectance spectra [15–18]. In the realm of noble-metal plasmonic sensors, various implementations of this approach have been studied [19–21]. Recently, the excitation of SLRs in arrays of ferromagnetic nickel nanoparticles was demonstrated [22]. The magneto-optical activity of an ordered ferromagnetic array is larger than that of randomly distributed nanoparticles, and it tunes sensitively with the period and symmetry of the lattice [22–24] or the size or shape of the nanoparticles [25]. The ability to compensate for intrinsic damping via the excitation of SLR modes offers new perspectives for refractive index sensing based on magnetoplasmonic architectures.

The integration of noble metals in hybrid magnetoplasmonic nanostructures can also reduce the linewidth of the spectral features in magneto-optical signals. Examples of such structures include noble metal-ferromagnetic multilayers [26–29], metallic sandwich-structure nanodisks [30, 31], and magnetic garnet films with integrated noble metal nanoparticles [32, 33] or gratings [34]. In all these realizations, the magnetic constituent is in direct contact with the noble metal. Dimer nanodisks wherein a dielectric layer separates the ferromagnet and noble metal [31, 35, 36] and composite arrays of pure ferromagnetic and noble metal nanoparticles [24] have also been explored.

Here, we present a direct experimental comparison between the refractive index sensing capabilities of LSPRs in pure Ni and Ni/SiO_2/Au dimer nanodisks and SLRs in ordered arrays of these two particle types. Changes in the dielectric environment are recorded by phase-sensitive detection of the magneto-optical signal. We test the sensing performance over a large refractive index range by performing measurements in air, water, and index-matching oil ($n = 1$, 1.33, and 1.52) and find that the FoM is enhanced by more than one order of magnitude in arrays of Ni/SiO_2/Au nanodisks compared to the other samples. We attribute the improved sensing performance to combined effects of near-field coupling between Ni and Au within the individual dimers and far-field diffractive coupling between the dimers.

2 Results and discussion

Ni nanodisks and cylindrical Ni/SiO_2/Au dimers were fabricated on glass substrates by electron beam lithography (see Section 4 for details). The particles are either distributed randomly (to probe the single-particle LSPR response) or in periodic square arrays with a lattice constant of 400 nm or 500 nm. The pure Ni nanodisks have a thickness of 30 nm and a diameter of 150 nm. The dimers consist of a 150-nm-diameter Au disk at the bottom and a slightly smaller Ni disk at the top. Both metals are 30 nm thick, and they are separated by 40 nm of SiO_2. For thinner spacer layers not discussed here, we measured a slightly reduced sensing performance because of resonance broadening in the strong-coupling regime. Figure 1A and B show scanning electron microscopy (SEM) images of a random distribution and an ordered array of dimer nanodisks.

The optical and magneto-optical spectra of the samples were measured in transmission geometry using a Faraday spectrometer (see Figure S1 of the Supplementary Material). The transmission configuration was intentionally chosen because it facilitates easier integration with microfluidics, lab on chip platforms, etc., in practical sensing applications. We used linearly polarized light at normal incidence and recorded the Faraday signal using polarizing optics, a photoelastic modulator, and lock-in amplification. During measurements, an out-of-plane magnetic field of ±400 mT was applied to saturate the magnetization of the Ni nanodisks. Here we focus on the use of Faraday rotation, i.e. the rotation of linear polarized light upon transmission, as sensitive probe for refractive index changes. Faraday ellipticity spectra of our samples are provided in the Supplementary Material.

LSPRs in an individual Ni/SiO_2/Au nanodisk can be interpreted as oscillating electric dipoles. Near the plasmon resonance condition, electric dipoles are directly excited in the Ni and Au nanodisks along the polarization axis of incident light ($d_{x\text{-}Ni}$ and $d_{x\text{-}Au}$ in the schematic illustration of Figure 1C). If the magnetization in Ni is oriented perpendicular to the disk by an external magnetic field, an orthogonal electric dipole is also excited along the y axis because of spin-orbit interactions ($d_{y\text{-}Ni}$). The magnitude of this so-called magneto-optical dipole is typically 100–500 times smaller than the electric dipole along the x axis [13]. Finally, near-field coupling between the Ni and Au nanodisks induces an orthogonal electric dipole in Au ($d_{y\text{-}Au}$). Taking phase retardation between the electric dipoles in the Ni (upper) and Au (lower) disks into account, the total electric dipole along x and y can be written as

$$\left|d_{x,y}\right|^2 = \left|d_{x,y-Ni} + d_{x,y-Au}\right|^2 = \left|d_{x,y-Ni}\right|^2 + \left|d_{x,y-Au}\right|^2 + 2\left|d_{x,y-Ni}\right|\left|d_{x,y-Au}\right|\cos\alpha_{x,y}, \quad (1)$$

where $\alpha_{x,y}$ indicates the phase difference between the electric dipoles in Ni and Au. The amplitude and phase relations of the four dipoles determine the optical and magneto-optical response of the Ni/SiO_2/Au dimer in

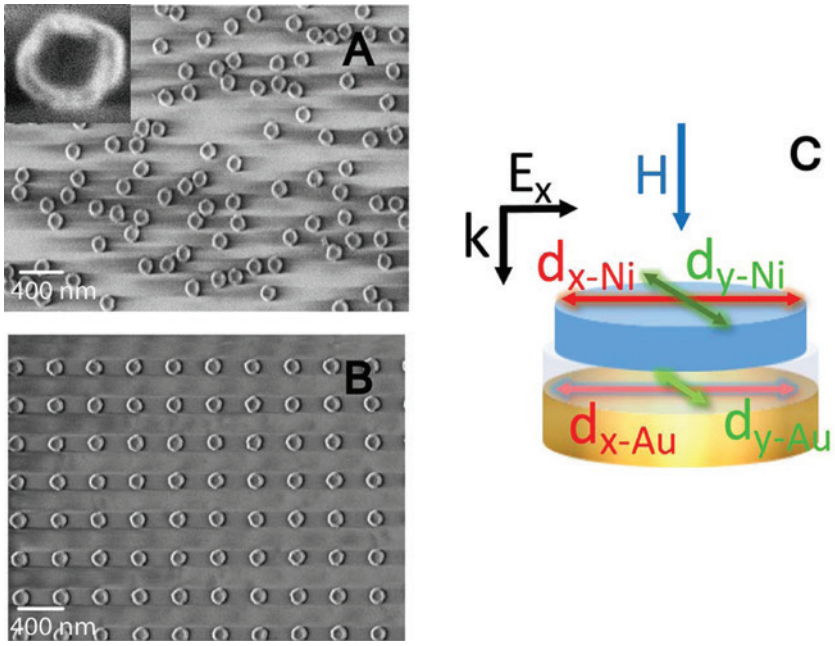

Figure 1: SEM images of samples with (A) a random distribution and (B) a periodic array of Ni/SiO_2/Au dimers ($a = 400$ nm). (C) Schematic illustration of the dimer structure. The Au and Ni nanodisk are 30 nm thick, and their diameter is 150 nm and about 130 nm, respectively. The two metals are separated by 40 nm SiO_2. Incident light with polarization along the x axis excites electric dipoles in Au and Ni ($d_{x\text{-}Ni}$ and $d_{x\text{-}Au}$) near the LSPR condition. Spin-orbit coupling induces an orthogonal dipole in Ni ($d_{y\text{-}Ni}$). Near-field coupling to this LSPR in Ni also excites an orthogonal dipole in Au ($d_{y\text{-}Au}$).

the far field [31, 35, 36]. In transmission geometry, the excitation of two orthogonal electric dipoles near the plasmon resonance condition causes the polarization of linearly polarized incident light to rotate and become elliptical. The Faraday angle is then defined as $\Phi = \theta + i\varepsilon$, where θ is the rotation and ε is the ellipticity of transmitted light.

We first discuss the sensing performance of random distributions of pure Ni nanoparticles and Ni/SiO_2/Au dimers. In this case, the optical transmission and Faraday spectra reflect the averaged response of the individual particles. Figure 2A shows the optical transmittance for pure Ni. A broad minimum in the transmittance spectrum is measured in air (black curve), water (blue curve), and index matching oil (red curve). The minimum, which we identify with the excitation of a LSPR mode, red-shifts when the refractive index of the surrounding medium is increased. Transmittance spectra for random Ni/SiO_2/Au dimers also show a red shift (Figure 2B). In this geometry, hybridization between a damped LSPR mode in Ni and a lower-loss resonance in Au narrows the plasmon peak. Faraday rotation data for both samples are shown in Figure 2C and D, respectively. The Faraday rotation θ changes sign at a characteristic wavelength λ_θ for all dielectric environments. We use phase-sensitive detection of this nulling condition as a measure of refractive index changes. Analogous to conventional noble-metal biosensors, the sensitivity of our magnetoplasmonic nanostructures is defined as $S = \Delta\lambda_\theta/\Delta n$. Comparing both data sets, we find larger spectral shifts of λ_θ and, thus, higher sensitivity for pure Ni nanoparticles compared to Ni/SiO_2/Au dimers (304 nm/RIU vs. 171 nm/RIU). However, the measurement accuracy depends also on the sharpness of the spectral feature that is used to track the refractive index change. In noble-metal plasmonic sensors, this is the resonance width. Since we infer changes in refractive index by monitoring the wavelength of zero Faraday rotation, the measurement accuracy depends on the slope $d\theta/d\lambda$ at λ_θ. According to literature, we therefore define the FoM of our magnetoplasmonic nanoparticles as $\mathrm{FoM} = S \times |d\theta/d\lambda|$ [37]. Fitting the slope of the Faraday rotation (Figure 2E) and multiplying by the sensitivity gives an average FoM of 1.4 mrad/RIU for the dimer structures. Despite better sensitivity, the FoM of the pure Ni nanoparticles is the same. Thus, for individual (i.e. non-interacting) nanoparticles, hybridization between the LSPRs of Ni and Au nanodisks enhances the measurement accuracy, but this improvement is entirely compensated by a reduction in sensor sensitivity.

Given that the sensitivity seems to be determined mostly by the individual nanoparticles, the best way to

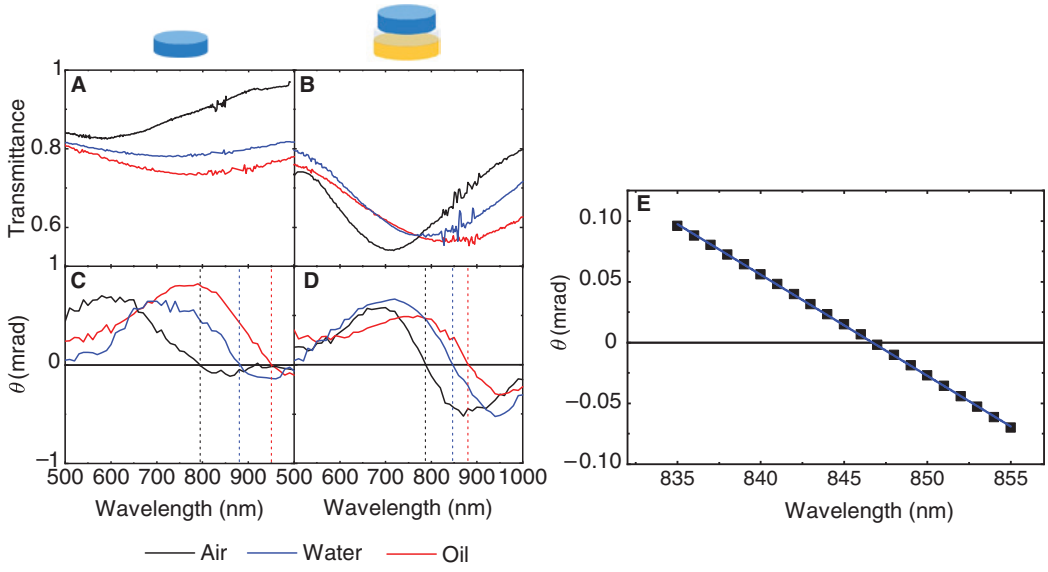

Figure 2: Optical and magneto-optical spectra of single nanoparticles.
(A, B) Transmittance and (C, D) Faraday rotation of a random distribution of Ni nanoparticles (left panels) and a random distribution of Ni/SiO_2/Au dimers (right panels), measured in air (black curves), water (blue curves), and index matching oil (red curves). The dashed vertical lines in (C) and (D) indicate the Faraday rotation nulling condition for the different dielectric environments. (E) Faraday rotation near the nulling condition ($\lambda_\theta = 847$ nm) for Ni/SiO_2/Au dimers in water. The linear fit to the experimental data gives $d\theta/d\lambda = -0.008$ mrad/nm. The noise level in the Faraday measurements in the spectral range shown is ~5 μrad, i.e. smaller than the square symbols in (E).

improve the sensing performance is by designing sharper spectral features, i.e. by increasing $d\theta/d\lambda$, with no or only limited reduction of S. This notion motivated us to turn our attention towards SLRs in periodic nanoparticle arrays. Figure 3 shows the transmittance and Faraday rotation of square arrays containing pure Ni nanoparticles (left) and Ni/SiO_2/Au dimers (right). SLRs arise from in-plane diffractive coupling of scattered fields from individual particles in the lattice. These collective modes can be described as the interference between a broad LSPR and a narrow resonance given by the diffracted order (DO) of the array. The <1,0> DO is normally observed as a sharp maximum in the transmittance spectrum at $\lambda_{DO} = na$. At slightly larger wavelength, the excitation of

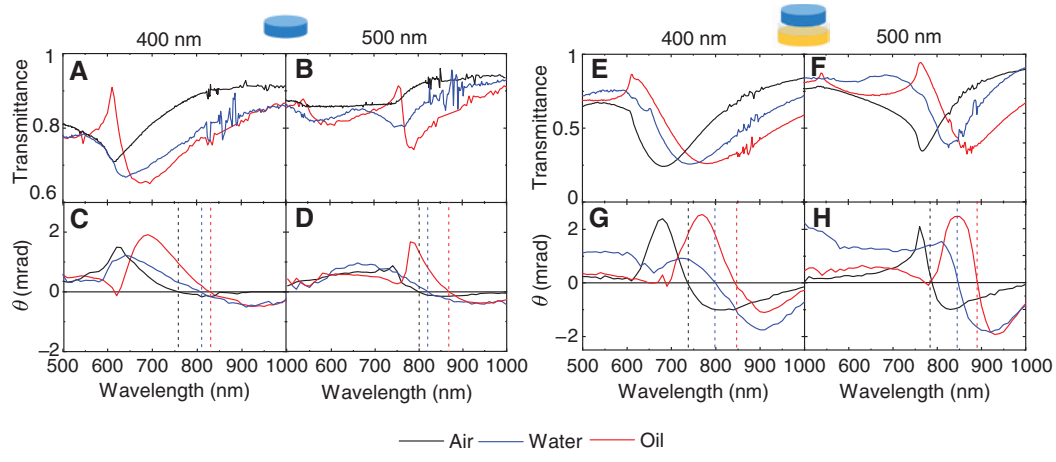

Figure 3: Optical and magneto-optical spectra of nanoparticle arrays.
(A, B, E, F) Transmittance and (C, D, G, H) Faraday rotation of periodic arrays of Ni nanoparticles (left panels) and periodic arrays of Ni/SiO_2/Au dimers (right panels), measured in air (black curves), water (blue curves), and index matching oil (red curves). Data for a lattice parameter of $a = 400$ nm and $a = 500$ nm are shown. The dashed vertical lines in the lower panels indicate the Faraday rotation nulling condition for the different dielectric environments.

an asymmetrical SLR mode causes an increase of optical absorption. The wavelength of maximum absorption (λ_{SLR}), i.e. minimal transmittance, and the SLR line shape depend sensitively on the lattice parameter and the particle diameter or, in other words, the difference between λ_{DO} and λ_{LSPR}. For noble-metal plasmonic nanoparticles, it has been shown that $\lambda_{DO}=\lambda_{SLR}$ maximizes the FoM [19].

If we first focus on the transmittance of Ni nanoparticle arrays (Figure 3A and B), we note that a clear DO resonance and narrow SLR mode are only measured if the particles are immersed in index matching oil. We attribute this observation to reflections from the interfaces between different refractive index layers in the air- and water-exposed systems, causing interferences that reduce constructive (SLR) or destructive (DO) far-field coupling between the nanoparticles of the array. For arrays with Ni/SiO_2/Au dimers, the situation is much better (Figure 3E and F). In this case, DO resonances and SLR modes are also visible in the transmittance spectra of the samples with inhomogeneous glass/air or glass/water dielectric environments. Thereby, even if in principle both systems would benefit from the excitation of SLRs, the incorporation of Au nanodisks in the dimer nanoparticles stabilizes collective lattice resonances via a strong enhancement of the scattered fields from the individual particles of the lattice (LSPRs). This ability to maintain SLRs over a wide refractive index range is essential for label-free biosensing.

The efficient excitation of a narrow SLR mode in Ni/SiO_2/Au dimer arrays also enhances the magneto-optical response and sharpens its spectral features. Compared to the pure Ni lattices (Figure 3C and D) or random Ni/SiO_2/Au dimers (Figure 2D), the Faraday rotation of the Ni/SiO_2/Au dimer arrays (Figure 3G and H) is larger, and the crossing of the nulling condition is much more abrupt. From the measurements we derive $S=191$ nm/RIU and $S=211$ nm/RIU for lattices with $a=400$ nm and $a=500$ nm, respectively, which is slightly larger than the sensitivity of individual dimer nanodisks. The big gain in magnetoplasmonic sensing performance is, however, due to a strong increase of $d\theta/d\lambda$ at λ_θ. As a result, the average FoM increases to 6.4 mrad/RIU for a lattice constant of $a=400$ nm and an even larger 15.1 mrad/RIU for $a=500$ nm. The latter value is more than one order of magnitude larger than that of random Ni/SiO_2/Au dimers. The improved sensing performance of the dimer array with larger lattice constant follows the design rule that states that sharper SLRs are attained when the spectral separation between λ_{DO} and λ_{LSPR} is reduced. For dimers in index matching oil $\lambda_{DO}(400\text{ nm})=608$ nm, $\lambda_{DO}(500\text{ nm})=760$ nm, and $\lambda_{LSPR}\approx 850$ nm (Figure 2B). These numbers suggest that the magneto-optical sensing performance can be improved further by adjusting the lattice parameter to a value where the condition $\lambda_{DO}=\lambda_{LSPR}$ is achieved. This ability to tailor the FoM via lattice design is particularly interesting for applications that require sensitive detection of refractive index changes around a specific value of n.

Table 1 summarizes the sensing parameters of all magnetoplasmonic samples. From the Faraday rotation data it is clear that pure Ni nanoparticle arrays exhibit a FoM that is comparable to random Ni nanoparticles or Ni/SiO_2/Au dimers. Strong enhancements of the sensing performance are only attained when Au nanodisks in the dimer structures assist in the excitation of narrow SLRs. We note that similar FoMs are achieved if the nulling condition of the Faraday ellipticity ($\lambda\varepsilon$) rather than the Faraday rotation (λ_θ) is used to measure refractive index changes. For an overview of Faraday ellipticity spectra and corresponding sensing parameters, we refer to the Supplementary Material. As a last consideration, we plot the wavelength of zero Faraday rotation and the FoM as a function of refractive index in Figure 4. From these data it is clear that the response of λ_θ to refractive index changes in the range $n=1.00$–1.52 is approximately linear and that strong enhancements of the FoM are realized over the entire

Table 1: Sensitivity (S), absolute value of $d\theta/d\lambda$, and FoM extracted from Faraday rotation measurements on all samples in air, water, and index matching oil.

	S (nm/RIU)	$\lvert d\theta/d\lambda\rvert$ (mrad/nm)			FoM (mrad/RIU)			$\overline{\text{FoM}}$
		Air	Water	Oil	Air	Water	Oil	(mrad/RIU)
Single Ni-Au dimer	171	0.010	0.008	0.007	1.7	1.4	1.2	1.4
Ni-Au lattice (400 nm)	191	0.040	0.020	0.040	7.3	3.8	7.6	6.2
Ni-Au lattice (500 nm)	211	0.060	0.070	0.090	12.7	13.7	19.0	15.0
Single Ni disc	304	0.004	0.006	0.004	1.2	1.7	1.2	1.4
Ni lattice (400 nm)	155	0.005	0.009	0.010	0.7	1.3	1.1	1.0
Ni lattice (500 nm)	130	0.007	0.010	0.010	0.9	1.3	1.6	1.3

The average sensing FoM measured over a large refractive index range of $n=1.00$–1.52 is shown on the right.

refractive index range for periodic arrays of Ni/SiO_2/Au dimers, especially if $a = 500$ nm.

The linear response of λ_θ to refractive index changes is explained by the fact that the plasmon resonance of the Ni nanoparticles occurs when the real part of the denominator in the expression of particle polarizability, $\varepsilon_{Ni}(\lambda) - 2\varepsilon_d$, is 0. Since the dielectric constant of Ni in the visible range (ε_{Ni}) varies approximately linearly with wavelength [38], the nulling condition of the Faraday rotation, which is directly linked to the spectral position of the plasmon resonance, shifts linearly with the dielectric constant of the surrounding environment (ε_d). Based on this linear response, we can provide a theoretical estimate of the ultimate refractometric sensing resolution (limit of detection) of our magnetoplasmonic structures. As a starting point, we consider the sensitivity of a magneto-optical measurement setup. With modulation-based detection and good polarizers, a Faraday rotation (or ellipticity) of ~10 nrad/$\sqrt{\text{Hz}}$ can be discerned from the noise level. The bandwidth of lock-in amplification is typically 1–10 Hz for integration times of 100 ms to 1 s typically utilized in measurements, which gives a detection sensitivity of 10–30 nrad. From this, the minimum detectable spectral shift of the nulling point ($\Delta\lambda_{\theta,\,\min}$) is estimated as (10–30 nrad)/($d\theta/d\lambda$). Using a value of $d\theta/d\lambda = 0.07$ mrad/nm for Ni/SiO_2/Au dimers in a lattice with $a = 500$ nm, we find $\Delta\lambda_{\theta,\,\min} = 1.4\text{–}4.2\times10^{-4}$ nm. Thus, for the same lattice, we derive a minimum detectable RIU ($\Delta\lambda_{\theta,\,\min}/S$) of 6×10^{-7} to 2×10^{-6} RIU. The estimated ultimate sensing resolution of our magnetoplasmonic structures is comparable to the best reported limit of detection of LSPR-based refractometric sensors, which is of the order of 10^{-7}–10^{-6} RIU [20, 39]. This is remarkable if one considers that only about 14% of the surface is covered by Ni/SiO_2/Au dimers. Detection of the nulling point in magneto-optical spectra does not require the subtraction of a measured baseline, which can be considered as an advantage over noble-metal SPP sensors because they do not exhibit such self-referencing capability. Since our measurement setup is not optimal (e.g. the supercontinuum laser is rather noisy), we also derive the limit of detection in our experiments. Based on a noise level of ~5 µrad in the Faraday measurements (Figure 2E), we find a detectable RIU of 4×10^{-4} for Ni/SiO_2/Au dimers in a lattice with a periodicity of 500 nm. This sensing resolution is comparable to the best results reported using noble-metal SLR structures [20]. Based on this analysis, we conclude that our work provides a clear path towards high-resolution refractive index sensing using magnetoplasmonics.

In our experiments, we systematically compare the sensing performance of magnetoplasmonic metamaterials and probe the influence of far-field diffractive coupling between nanoparticles in an ordered array and the effect of near-field coupling between Ni and Au nanodisks at the single particle level. While the FoMs of our structures do not outperform those of plasmonic sensors based on noble metals (see e.g. Ref. [20]), one should be careful in comparing FoM numbers directly because definitions vary. Importantly, the limit of detection of a refractive index sensor does not only depend on the FoM but also on the measurement method (see discussion above). In the analysis of our results, we considered raw magneto-optical measurement data without any normalization or other post-processing. The key advantage of our magnetoplasmonic approach is the combination of intrinsic phase-sensitivity and the tracking of a well-defined nulling condition (Faraday rotation or ellipticity), enabling refractometric sensing with very small detection limits.

On a more general level, we also find it instructive to compare magnetoplasmonic sensing concepts that exploit SPPs in metallic multilayers [40] and our SLR-based ferromagnetic nanoparticle arrays. In the Kretschmann configuration, the sensing FoM depends on a magneto-optical modulation of the SPP wave vector and the SPP propagation length. The same holds for noble metal/magneto-optical dielectric bilayers [37]. In both types of structures, the SPP propagation length, and thus intrinsic or radiative losses,

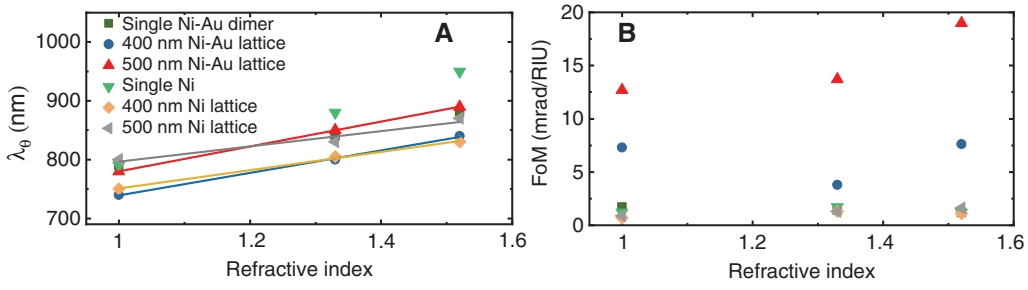

Figure 4: Summary of sensing performance of all magnetoplasmonic samples.
(A) Wavelength of zero Faraday rotation (λ_θ) and (B) FoM as a function of the refractive index of the embedding medium.

determines the spectral width of the SPP resonance and the sensing FoM. In contrast, the resonance width of SLR modes in magnetoplasmonic nanoparticle arrays are not strictly limited by high ohmic losses in the ferromagnets. Here, the shape and size of the individual nanoparticles and lattice parameters can be utilized to design sharp resonances in magneto-optical spectra [22–25]. The improved sensing performance of arrays with a lattice constant of 500 nm compared to those with $a = 400$ nm in this study is a clear manifestation of this effect.

3 Conclusions

We have shown that ordered arrays of Ni/SiO_2/Au dimer nanodisks offer sensitive magnetoplasmonic detection of refractive index changes. Whereas the sensing performances of random distributions of pure Ni nanoparticles and Ni/SiO_2/Au dimers are similar, the integration of Au at the single-particle level of ordered dimer arrays is instrumental in establishing robust and spectrally narrow SLRs in non-uniform dielectric environments. As a result, the sensing FoM of dimer arrays is drastically enhanced compared to that of pure Ni nanoparticle arrays. The improved performance is mainly caused by the sharp spectral features of the SLR mode, enabling more accurate measurements of the Faraday nulling condition. Tuning of the SLR resonance condition via a variation of the lattice constant provides a versatile way of maximizing the magnetoplasmonic sensing FoM for specific applications.

4 Methods

We prepared the samples on glass substrates using electron beam lithography. After spin-coating a polymethyl methacrylate (PMMA) layer and baking at 180°C for 1 min, the pattern was defined by exposing the resist layer to the electron beam. We developed the PMMA in a 1:3 methyl isobutyl ketone (MIBK):isopropanol (IPA) solution. Samples with pure Ni nanoparticles were fabricated by magnetron sputtering of a 30-nm-thick Ni layer and lift-off. For dimer samples, we first grew a 30-nm-thick Au layer using electron beam evaporation on a 1-nm-thick Ti adhesion layer. After this, the samples were transferred to a magnetron sputtering system for the deposition of 40 nm SiO_2 (radio frequency sputtering from a SiO_2 target) and the growth of 30 nm of Ni. We used SEM and atomic force microscopy to determine the particle diameters. The disks that were in contact with the glass substrate (Ni in pure Ni nanoparticles and Au in the dimers) had a diameter of 150 nm. The diameter of the Ni nanodisks in the dimer nanoparticles was about 130 nm.

Optical transmission and Faraday rotation and ellipticity measurements were conducted with a Faraday spectrometer. The setup consisted of a broadband supercontinuum laser (SuperK EXW-12 laser with acousto-optical filter from NKT Photonics, Denmark), polarizing (Glann-Thompson prism from CVI MellesGriot, Netherlands) and focusing optics, a photoelastic modulator (Hinds Instruments I/FS50, Portland, OR, USA), and a photodetector. The wavelength of the laser was tuned between 500 nm and 1000 nm. We used linear polarized light at normal incidence. During measurements, a ±400 mT field from an electromagnet (model 3470 from GMW, San Carlos, CA, USA) switched the magnetization of the Ni nanodisks between the two perpendicular directions. The Faraday rotation and ellipticity were simultaneously recorded by lock-in amplification of the modulated signal at 50 kHz and 100 kHz. To measure the sensitivity and FoM of the nanoparticle samples over a large refractive index range, we performed measurements in air, water, and index-matching oil ($n = 1$, 1.33, and 1.52). A front cover glass was used to embed the nanoparticles in water and oil. As a reference, we measured the transmittance of the samples in an area without nanoparticles.

Acknowledgments: This work was supported by the Aalto Centre for Quantum Engineering. Lithography was performed at the Micronova Nanofabrication Centre, supported by Aalto University. P.V. acknowledges support from the Spanish Ministry of Economy, Industry and Competitiveness under the Maria de Maeztu Units of Excellence Programme – MDM-2016-0618.

References

[1] Homola J, Yee SS, Gauglitz G. Surface plasmon resonance sensors: review. Sens Act B 1999;54:3–15.
[2] Anker JN, Paige Hall W, Lyandres O, Shah NS, Zhao J, Van Duyne RP. Biosensing with plasmonic nanosensors. Nat Mater 2008;7:442–53.
[3] Stewart ME, Anderton CR, Thompson LB, et al. Nanostructured plasmonic sensors. Chem Rev 2008;108:494–521.
[4] Mayer KM, Hafner JH. Localized surface plasmon resonance sensors. Chem Rev 2011;111:3828–57.
[5] Špačková B, Wrobel P, Bocková M, Homola J. Optical biosensors based on plasmonic nanostructures: a review. Proc IEEE 2016;104;2380–408.
[6] Dmitriev A, Hägglund C, Chen S, et al. Enhanced nanoplasmonic optical sensor with reduced substrate effect. Nano Lett 2008;8:3893–8.

[7] Svedendahl M, Dmitriev A, Käll M. Refractometric sensing using propagating versus localized surface plasmons: a direct comparison. Nano Lett 2009;9:4428–33.
[8] Otte MA, Sepúlveda B, Ni W, Pérez Juste J, Liz-Marzán LM, Lechuga LM. Identification of the optimal spectral region for plasmonic and nanoplasmonic sensing. ACS Nano 2009;4:349–57.
[9] Lodewijks K, Van Roy W, Borghs G, Lagae L, Van Dorpe P. Boosting the figure-of-merit of LSPR-based refractive index sensing by phase-sensitive measurements. Nano Lett 2012;12:1655–9.
[10] Chen J, Albella P, Pirzadeh Z, et al. Plasmonic nickel nanoantennas. Small 2011;7:2341–7.
[11] Bonanni V, Bonetti S, Pakizeh T, et al. Designer magnetoplasmonics with nickel nanoferromagnets. Nano Lett 2011;11:5333–8.
[12] Grunin AA, Zhdanov AG, Ezhov AA, Ganshina EA, Fedyanin AA. Surface-plasmon-induced enhancement of magneto-optical Kerr effect in all-nickel subwavelength nanogratings. Appl Phys Lett 2010;97:261908.
[13] Maccaferri N, Berger A, Bonetti S, et al. Tuning of magneto-optical response of nanosized ferromagnetic Ni disks using the phase of localized plasmons. Phys Rev Lett 2013;111:167401.
[14] Maccaferri N, Gregorczyk KE, de Oliveira TVAG, et al. Ultrasensitive and label-free molecular-level detection enabled by light phase control in magnetoplasmonic nanoantennas. Nat Commun 2015;6:6150.
[15] Auguié B, Barnes WL. Collective resonances in gold nanoparticle arrays. Phys Rev Lett 2008;101:143902.
[16] Luk'yanchuk B, Zheludev NI, Maier SA, et al. The Fano resonance in plasmonic nanostructures and metamaterials. Nat Mater 2010;9:707–15.
[17] Halas NJ, Lal S, Chang WS, Link S, Nordlander P. Plasmons in strongly coupled metallic nanostructures. Chem Rev 2011;6:3913–61.
[18] Meinzer N, Barnes WL, Hooper IR. Plasmonic meta-atoms and metasurfaces. Nat Photonics 2014;8:889–98.
[19] Offermans P, Schaafsma MC, Rodriguez SRK, et al. Universal scaling of the figure of merit of plasmonic sensors. ACS Nano 2011;5:5151–7.
[20] Shen Y, Zhou J, Liu T, et al. Plasmonic gold mushroom arrays with refractive index sensing figures of merit approaching the theoretical limit. Nat Commun 2013;4:2381.
[21] Lodewijks K, Ryken J, Van Roy W, Borghs G, Lagae L, Van Dorpe P. Tuning the Fano resonance between localized and propagating surface plasmon resonances for refractive index sensing applications. Plasmonics 2013;8:1379–85.
[22] Kataja M, Hakala TK, Julku A, Huttunen MJ, van Dijken S, Törmä P. Surface lattice resonance and magneto-optical response in magnetic nanoparticle arrays. Nat Commun 2015;6:7072.
[23] Kataja M, Pourjamal S, van Dijken S. Magnetic circular dichroism of non-local surface lattice resonances in magnetic nanoparticle arrays. Opt Express 2016;24:3562–71.
[24] Kataja M, Pourjamal S, Maccaferri N, et al. Hybrid plasmonic lattices with tunable magneto-optical activity. Opt Express 2016;24:3652–62.
[25] Maccaferri N, Bergamini L, Pancaldi M, et al. Anisotropic nanoantenna-based magnetoplasmonic crystals for highly enhanced and tunable magneto-optical activity. Nano Lett 2016;16:2533–42.
[26] Safarov VI, Kosobukin VA, Hermann C, Lampel G, Peretti J, Marlière C. Magneto-optical effects enhanced by surface plasmons in metallic multilayer films. Phys Rev Lett 1994;73:3584–7.
[27] Ferré J, Pénissard G, Marlière C, Renard D, Beauvillain P, Renard JP. Magneto-optical studies of Co/Au ultrathin metallic films. Appl Phys Lett 1990;56:1588–90.
[28] Ferreiro-Vila E, González-Díaz JB, Fermento R, et al. Intertwined magneto-optical and plasmonic effects in Ag/Co/Ag layered structures. Phys Rev B 2009;80:125132.
[29] Armelles G, González-Díaz JB, García-Martín A, et al. Localized surface plasmon resonance effects on the magneto-optical activity of continuous Au/Co/Au trilayers. Opt Express 2008;16:16104–12.
[30] González-Díaz JB, García-Martín A, García-Martín JM, et al. Plasmonic Au/Co/Au nanosandwiches with enhanced magneto-optical activity. Small 2008;4:202–5.
[31] Banthí JC, Meneses-Rodríguez D, García F, et al. High magneto-optical activity and low optical losses in metal-dielectric Au/Co/Au-SiO_2 magnetoplasmonic nanodisks. Adv Mater 2012;24:OP36–41.
[32] Fujikawa R, Baryshev AV, Kim J, Uchida H, Inoue M. Contribution of the surface plasmon resonanceto optical and magneto-optical properties of a Bi:YIG-Au nanostructure. J Appl Phys 2008;103:07D301.
[33] Tomita S, Kato T, Tsunashima S, Iwata S, Fujii M, Hayashi S. Magneto-optical Kerr effects of yttrium-irongarnet thin films incorporating gold nanoparticles. Phys Rev Lett 2006;96:167402.
[34] Belotelov VI, Akimov IA, Pohl M, et al. Enhanced magneto-optical effects in magnetoplasmonic crystals. Nat Nanotechnol 2011;6:370–6.
[35] de Sousa N, Froufe-Pérez LS, Armelles G, et al. Interaction effects on the magneto-optical response of magnetoplasmonic dimers. Phys Rev B 2014;89:205419.
[36] Armelles G, Cebollada A, García-Martín A, et al. Mimicking electromagnetically induced transparency in the magneto-optical activity ofmagnetoplasmonic nanoresonators. Opt Express 2013;21:27356–70.
[37] Qin J, Deng L, Xie J, Tang T, Bi L. Highly sensitive sensors based on magneto-optical surface plasmon resonance in Ag/CeYIG heterostructures. AIP Adv 2015;5:017118.
[38] Johnson PB, Christy, RW. Optical constants of transition metals: Ti, V, Cr, Mn, Fe, Co, Ni, and Pd. Phys Rev B 1974;9:5056–70.
[39] Homola, J. Surface plasmon resonance sensors for detection of chemical and biological species. Chem Rev 2008;108: 462–93.
[40] Martín-Becerra D, Temnov VV, Thomay T, et al. Spectral dependence of the magnetic modulation of surface plasmon polaritons in noble/ferromagnetic/noble metal films. Phys Rev B 2012:86:035118.

Supplemental Material: The online version of this article offers supplementary material (https://doi.org/10.1515/nanoph-2018-0013).